A

K_I and K_{II} Solutions for an Edge-Cracked Beam

A.1 An Expression for K_I

An expression of K_I for an edge-cracked beam is originally given in [17] as

$$K_I = \sqrt{\pi a t} f_o(a)\{\sigma(0) + \frac{2}{\pi}\int_0^a (1-z)^2 cos^{-1}[\frac{(1-a)z}{a(1-z)}][1 - \frac{z}{a}G(a)]\frac{\partial \sigma(z)}{\partial z}dz\} \tag{A.1}$$

in which [93]

$$f_o(a) = \left\{\frac{0.752 + 2.017a + 0.369[1-\sin(\pi a/2)]^2}{\cos(\pi a/2)}\right\}\sqrt{\frac{2}{\pi a}\tan(\frac{\pi a}{2})} \tag{A.2}$$

and

$$G(a) = \alpha(1-7a)(1-a)^5$$

where $\alpha \approx 0.12/1.12 = 3/28$, a and z are the crack length and distance normalized by thickness. Equation (A.1) is only convenient when the derivative of the stress field can readily be evaluated. Computer programs written in C are provided in Appendix C to evaluate the derivative of Legendre and Chebyshev polynomials. For a general stress field we may rewrite Eq. (A.1) as

$$K_I = \sqrt{\pi a t}(\frac{2}{\pi}) f_o(a)\int_0^a \left\{(1-z)(2 + G/a - 3zG/a)cos^{-1}[\frac{(1-a)z}{a(1-z)}] + \frac{(1-a)(1-zG/a)}{a\sqrt{1-\left[\frac{(1-a)z}{a(1-z)}\right]^2}}\right\}\sigma(z)dz \tag{A.3}$$

One problem with Eq. (A.3) is that it is not well defined for an edge crack in semi-infinite plane. It would be convenient to use a single solution to

compute K_I for the whole range of the thickness. Letting $v = z/a$, the first term of the integrand of Eq. (A.3) becomes

$$\int_0^1 (1 - va)(2a + G - 3Gva) \cos^{-1}(\frac{(1-a)v}{1-av})\sigma(va)dv$$

and the second term becomes

$$\int_0^1 \frac{(1-a)(1-Gv)}{\sqrt{1-[\frac{(1-a)v}{1-av}]^2}}\sigma(va)dv$$

Although evaluation of derivative is no longer needed, the second term contains a singularity at $v = 1$ that makes an accurate numerical integration difficult. To eliminate the singularity, we rewrite it as

$$\int_0^a \frac{(1-a)(1-Gv)}{\sqrt{1-(\frac{(1-a)v}{1-av})^2}}\sigma(va)dv$$
$$= \int_0^{\pi/2} \frac{(1-a)^2[1-a+(a-G)\sin u]}{(1-a+a\sin u)^3}\sigma(\frac{a\sin u}{1-a+a\sin u})du \qquad \text{(A.4)}$$

The final expression now takes the following form

$$K_I = \sqrt{\pi at}(\frac{2}{\pi})f_o(a)\left\{\int_0^1 (1-va)(2a+G-3Gva)\cos^{-1}[\frac{(1-a)v}{1-av}]\sigma(va)dv\right.$$
$$\left. + \int_0^{\pi/2} \frac{(1-a)^2[1-a+(a-G)\sin u]}{(1-a+a\sin u)^3}\sigma(\frac{a\sin u}{1-a+a\sin u})du\right\} \qquad \text{(A.5)}$$

A.2 An Expression for K_{II}

The expression for K_{II} takes a similar form as that for K_I, i.e.,

$$K_{II} = \sqrt{\pi at}g_o(a)\left\{[\tau(0)]\right.$$
$$\left. +(\frac{2}{\pi})\int_0^a (1-z)\cos^{-1}(\frac{F(a)z}{1-z})[1-\frac{z}{a}H(a)]\frac{\partial\tau(z)}{\partial z}dz\right\} \qquad \text{(A.6)}$$

where [123]

$$g_o(a) = (1.122 - 0.561a + 0.085a^2 + 0.18a^3)/(1-a)^{1/2}$$

and

$$H(a) = \alpha(1 - 2.5a)(1 - a)$$

B

Stresses Due to Point Forces

The normal stress on the central plane of the strip due to a pair of horizontal or vertical point loads acting symmetrically at distance s on the upper edge of a strip is given respectively by

$$\begin{aligned}\frac{F}{\pi t}S(s,x) &= \frac{F}{\pi t}\{\frac{4s^3}{(s^2+x^2)^2} + \int_0^\infty [(\alpha-1)G(\alpha,x) + \alpha H(\alpha,x)]e^{-\alpha}\sin(\alpha s)d\alpha\} \\ \frac{Q}{\pi t}T(s,x) &= \frac{Q}{\pi t}\{\frac{4s^2x}{(s^2+x^2)^2} + \int_0^\infty [\alpha G(\alpha,x) + (\alpha+1)H(\alpha,x)]e^{-\alpha}\cos(\alpha s)d\alpha\}\end{aligned} \tag{B.1}$$

where

$$\begin{aligned}G(\alpha,x) = \\ \frac{\alpha(1-x)\sinh(\alpha x) - 2\cosh[(\alpha(1-x)] + \alpha x\sinh[\alpha(1-x)] - 2\cosh(\alpha x)}{\sinh(\alpha)+\alpha} \\ + \frac{\alpha(1-x)\sinh(\alpha x) + 2\cosh[\alpha(1-x)] - \alpha x\sinh[\alpha(1-x)] - 2\cosh(\alpha x)}{(\sinh(\alpha)-\alpha)}\end{aligned}$$

$$\begin{aligned}H(\alpha,x) = \frac{\alpha(1-x)\cosh(\alpha x) - \sinh[\alpha(1-x)] + \alpha x\cosh[\alpha(1-x)] - \sinh(\alpha x)}{\sinh(\alpha)+\alpha} \\ + \frac{\alpha(1-x)\cosh(\alpha x) + \sinh[\alpha(1-x)] - \alpha x\cosh[\alpha(1-x)] - \sinh(\alpha x)}{\sinh(\alpha)-\alpha}\end{aligned}$$

Replacing x by $1-x$ in Eq. (B.1) leads to expressions for the normal stresses due to point loads acting on the lower edge of the strip.

For strain computation the partial derivative with respect to s gives

$$\begin{aligned}\frac{\partial S(s,x)}{\partial s} &= \frac{4s^2(3x^2-s^2)}{(s^2+x^2)^3} + \int_0^\infty [(\alpha-1)G(\alpha,x) + \alpha H(\alpha,x)]e^{-\alpha}\alpha\cos(\alpha s)d\alpha \\ \frac{\partial T(s,x)}{\partial s} &= \frac{8sx(x^2-s^2)}{(s^2+x^2)^3} - \int_0^\infty [(\alpha-1)G(\alpha,x) + \alpha H(\alpha,x)]e^{-\alpha}\alpha\sin(\alpha s)d\alpha\end{aligned} \tag{B.2}$$

for the horizontal and vertical point loads respectively.

For a pair of horizontal point loads on the lower edge

$$\frac{\partial S(1-x,s)}{\partial s} = \frac{4s^2[3(1-x)^2 - s^2]}{[s^2 + (1-x)^2]^3} + \int_0^\infty [(\alpha - 1)G(\alpha, 1-x) + \alpha H(\alpha, 1-x)]e^{-\alpha}\alpha \cos(\alpha s)d\alpha \quad \text{(B.3)}$$

which, at $s = 0$, reduces to

$$\frac{\partial S(1-s,x)}{\partial s}_{|s=0} = \int_0^\infty [(\alpha - 1)G(\alpha, 1-x) + \alpha H(\alpha, 1-x)]e^{-\alpha}\alpha d\alpha \quad \text{(B.4)}$$

To simplify the computation of Eq. (B.4) we express it in terms of a Legendre polynomial expansion

$$\frac{\partial S(s,1-x)}{\partial s}_{s=0} = \frac{12}{\pi}L_1(x) + \sum_{i=2}^{n} b_i \; L_i(x) \quad \text{(B.5)}$$

For $n = 15$ the coefficients b_i are tabulated in Table B.1.

Table B.1. Coefficients of Legendre series for approximation of Eq. (B.4)

i	b_i	i	b_i
2	-2.263850148374880e-001	9	2.430841835789998e-005
3	1.479050903091393e-001	10	-5.110357726474321e-006
4	-2.610313660458882e-002	11	1.106426725616064e-006
5	9.050406633413190e-003	12	-2.283685583449879e-007
6	-1.860168650373919e-003	13	4.738479609037172e-008
7	4.934447220567688e-004	14	-9.591872844605387e-009
8	-1.045400500176257e-004	15	1.935575313092089e-009

C

C Subroutines for the Calculation of Polynomial Series

C.1 Chebyshev Polynomials

/* This program uses the recurrence relation to compute the value of an n^{th} order Chebyshev polynomial series for a given value of x.
Input variables:
x - independent variable with $0 \leq x \leq 1$;
n - order of the series;
a[] - coefficients vector.*/

```
double ChbySum(double x,int n,double a[])
{
    double v0,v1,v2,sum;
    int j;
    sum = a[0];
    x = 2.*x-1.;
    if(n>0)
    {
        v0 = 1.;
        v1 = x;
        sum += a[1]*v1;
        for(j=2; j≤n; ++j)
        {
            v2 = 2*x*v1-v0;
            sum = sum+a[j]*v2;
            v0 = v1;
            v1 = v2;
        }
        return sum;
    }
    return sum;
}
```

```
/* This program uses the recurrence relation to compute the value of an
n^th order Chebyshev polynomial for a given value of x.
    Input variables:
        x - independent variable with 0 ≤ x ≤ 1;
        n - order of the polynomial;*/

double ChbyVal(double x,int n)
{
    double v0,v1,v2;
    int j;
    if(n>0)
    {
        x = 2.*x-1.;
        v0 = 1.;
        v1 = x;
        for(j=2; j≤n; ++j)
        {
            v2 = 2*x*v1-v0;
            v0 = v1;
            v1 = v2;
        }
        return v1;
    }
    return 1.;
}

/* This program uses the recurrence relation to compute the value of the
first derivative of an n^th order Chebyshev polynomial for a given value of x,
which can be used directly in Eq. (A.1).
    Input variables:
        x - independent variable with 0 ≤ x ≤ 1;
        n - order of the polynomial;
This routine can be efficiently used in the numerical integration of the LEFM
solution.*/

double ChbyDVal(double x,int n)
{
    double v0,v1,v2;
    int j;
    x = 2.*x-1.;
    if(n>0)
    {
        n−−;
        if(n>0)
```

```
        {
            v0 = 1.;
            v1 = 2*x;
            for(j=2; j≤n; ++j)
            {
                v2 = 2*x*v1-v0;
                v0 = v1;
                v1 = v2;
            }
            return v1*(n+1);
        }
        return 1.;
    }
    return 0.;
}
```

C.2 Legendre Polynomials

```
/* This program uses the recurrence relation to compute the value of an n^th
order Legendre series for a given value of x.
    Input variables:
        x - independent variable with 0 ≤ x ≤ 1;
        n - order of the series;
        a[] - coefficients vector.
A continuous normal residual stress distribution can be obtained by setting
a[0] and/or a[1] to zero.*/
double LegenSum(double x,int n,double a[])
{
    double v0,v1,v2,sum;
    int j;
    sum = a[0];
    x = 2.*x-1.;
    if(n>0)
    {
        v0 = 1.;
        v1 = x;
        sum += a[1]*v1;
        for(j=2; j≤n; ++j)
        {
            v2 = (2*j-1.)*x*v1-(j-1.)*v0/j;
            sum = sum+a[j]*v2;
            v0 = v1;
            v1 = v2;
        }
        return sum;
    }
    return sum;
}

/* This program uses the recurrence relation to compute the value of an
n^th order Legendre polynomial for a given value of x.
    Input variables:
        x - independent variable with 0 ≤ x ≤ 1;
        n - order of the polynomial;*/
double LegenVal(double x,int n)
{
    double v0,v1,v2;
    int j;
    if(n>0)
    {
        x = 2.*x-1.;
```

```
        v0 = 1.;
        v1 = x;
        for(j=2; j≤n; ++j)
        {
            v2 = (2*j-1.)*x*v1-(j-1.)*v0/j;
            v0 = v1;
            v1 = v2;
        }
        return v1;
    }
    return 1.;
}
```

/* This program returns the value of the first derivative of an n^{th} order Legendre polynomial for a given value of x, which can be used directly in Eq. (A.1).

Input variables:

x - independent variable with $0 \leq x \leq 1$;

n - order of the polynomial;

This routine can be efficiently used in the numerical integration of the LEFM solution.*/

```
double LegenDVal(double x,int n)
{
    double v0,v1,v2,d0,d1;
    int j;
    x = 2.*x-1.;
    if(n>0)
    {
        v0 = 1.;
        v1 = x;
        d0 = 1.;
        d1 = 3.*x;
        for(j=2; j≤n; ++j)
        {
            v2 = (2*j-1.)*x*v1-(j-1.)*v0/j;
            d1 = j*v1+x*d0;
            v0 = v1;
            v1 = v2;
            d0 = d1;
        }
        return d0;
    }
    return 0.;
}
```

C.3 Jacobi Polynomials

A Jacobi polynomial series can be used to represent a continuous shear stress which vanishes at free surfaces ($x = 0$ and $x = 1$), i.e.,

$$\tau(x) = x(1-x)\sum_{i=1}^{n} A_i J_i(x)$$

A residual shear stress is obtained when $A_1 = 0$

```
/* This program uses the recurrence relation to compute the value of an
n^th order Jacobi polynomial for a given value of x.
    Input variables:
        x - independent variable with 0 ≤ x ≤ 1;
        n - order of the polynomial;
*/
double JacoVal(double x,int n)
{
    double v0,v1,v2;
    int j;
    x = 2.*x-1.;
    if(n>0)
    {
        v0 = 1.;
        v1 = 2.*x;
        for(j=2; j≤n; ++j)
        {
            v2 = ((2*j+1)*(j+1)*x*v1-j*(j+1)*v0)/(j*(2+j));
            v0 = v1;
            v1 = v2;
        }
        return v1;
    }
    return 1.;
}

/* This program returns the sum of an n^th order Jacobi polynomial series
for a given value of x.
    Input variables:
        x - independent variable with 0 ≤ x ≤ 1;
        n - order of the polynomial;
*/
double JacoSum(double x,int n,double A[])
{
    double v0,v1,v2,sum;
```

```
    int j;
    x = 2.*x-1.;
    if(n>0)
    {
        v0 = 1.;
        v1 = 2.*x;
        for(j=2; j≤n; ++j)
        {
            v2 = ((2*j+1)*(j+1)*x*v1-j*(j+1)*v0)/(j*(2+j));
            v0 = v1;
            v1 = v2;
        }
        return v1;
    }
    return 1.;
}
```

D

K_I Solution for an Edge-Cracked Disk

The K_I solution for an edge-cracked disk due to an arbitrary loading on crack faces has been studied by several authors using weight functions [132, 49]. As pointed out by Schindler [118], for a deep crack subjected to self-equilibrating stresses, the polynomial approximation proposed by Petroski and Achenbach [92] is no longer applicable because of the inconsistency between the far-field conditions and the near crack tip functions used in the polynomial. To overcome this problem, a new weight function is recently proposed by Schindler [118] which leads to an improved result for deep cracks. Here we take an alternative approach to obtain a weight function based on an asymptotic interpolation of the solutions for a very shallow and a very deep crack.

D.1 Analysis

Consider a disk of diameter D with an edge crack of size a normalized by the diameter shown in Fig. D.1. For a very shallow crack the K_I solution reduces to that of for an edge crack in a semi-infinite plane. For an arbitrary normal stress $\sigma(x)$ on the crack faces, the solution has been given in [17] as

$$K_I = 1.12\sigma\sqrt{\pi a D}\int_0^a \frac{\partial}{\partial x}\left[-(\frac{2}{\pi})\cos^{-1}(\frac{x}{a})(1-\frac{\alpha x}{a})\right]\sigma(x)dx \qquad \text{(D.1)}$$

in which x is the distance taken from the crack mouth, as shown in Fig. D.2, and α a constant approximately equal to 3/28.

Following the same consideration for an edge-cracked strip [17], the solution for an arbitrary normal stress acting on the faces of a very deep crack in a disk may be given by

$$K_I = \sqrt{\pi a D} f_0(a) 2\int_0^1 (1-z)\sigma(z)dz \qquad \text{(D.2)}$$

where z is the normalized distance x/D. The K_I solution $f^0(a)$ for a uniform normal traction on crack faces shown in Fig. D.1 is given in a very simple

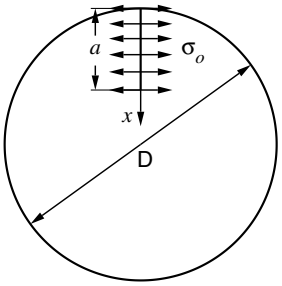

Fig. D.1. A disk of diameter D with an edge crack of size a subjected to a uniform stress σ_o on crack faces.

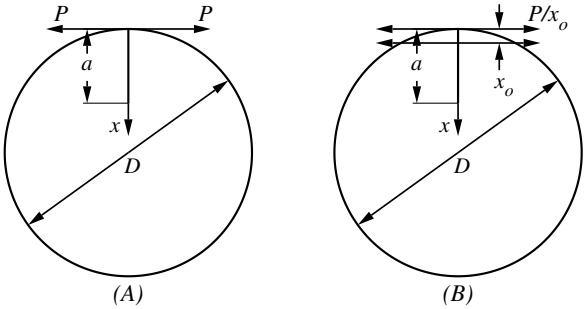

Fig. D.2. A disk of diameter $D = 1$ with an edge crack of size a subjected to a pair of forces P on the crack mouth (a), which is approximated by a strip load of P/x_o in (b).

form [49] as

$$f_0(a) = 1.12(1-a)^{-3/2} \tag{D.3}$$

To obtain a solution of K_I for all values of a, the corresponding expression based on an asymptotic interpolation may be written as

$$K_I = \sigma\sqrt{\pi a D} f_0(a) f(a) \tag{D.4}$$

where σ is a reference stress and

$$f(a) = \int_0^a \frac{\partial}{\partial z} \left\{ (1-(1-z)^2(\frac{2}{\pi}) \cos^{-1} \left[\frac{z(1-a)}{(1-z)a} \right] H(z,a) \right\} \frac{\sigma(z)}{\sigma} dz \quad \text{(D.5)}$$

Eq. (D.4) reduces to Eq. (D.1) or (D.2) only if the asymptotic interpolation function $H(z,a)$ satisfies

$$\lim_{d \to \inf} H(z,a) = 1 - \alpha \frac{x}{a} \lim_{a \to d} H(z,a) = 1 \quad \text{(D.6)}$$

As will be shown later, the simplest form for $H(z,a)$ may be given by

$$H(z,a) = 1 - \alpha z(1-a)/a \quad \text{(D.7)}$$

To show that Eq. (D.7) leads to an excellent approximation of the exact K_I solution, we consider the solution for a pair of point forces acting at the edge of the crack as shown in Fig. D.2-a. For simplicity without losing generality, we take D = 1 in the derivation that follows. The exact solution of K_I in this case is given in [132] as

$$K_I = \frac{P}{\sqrt{\pi a}} \frac{2.5935 + 4.4533a}{(1-a)^{3/2}} \quad \text{(D.8)}$$

Replacing the stress field in Eq. (D.5) by a strip load P/x_o shown in Fig. D.2-b, Eq. (D.4), when combine with Eq. (D.7), becomes

$$K_I = P\sqrt{\pi a} \frac{f_0(a)}{x_o} \left\{ 1 - (1-x_o)^2(\frac{2}{\pi}) \cos^{-1} \left[\frac{x_o(1-a)}{a(1-x_o)} \right] [1 - \frac{\alpha x_o}{a}(1-a)] \right\} \quad \text{(D.9)}$$

Taking the limit of x_o approaching zero gives

$$K_I = \frac{1.12P}{(1-a)^{3/2}} \sqrt{\frac{\pi}{a}} [\alpha + \frac{2}{\pi} + a(2 - \alpha - \frac{2}{\pi})] = \frac{P}{\sqrt{\pi a}} \frac{2.6170 + 4.4202a}{(1-a)^{3/2}} \quad \text{(D.10)}$$

The maximum difference between Eq. (D.10) and Eq. (D.8) is only 0.9%. Turning to Eq. (D.7), we could also express the asymptotic interpolation function in a more general form. That is, for $D = 1$,

$$H(z,a) = 1 - \alpha z(1-a)(1 + \sum_{i=1}^{n} c_i a^i)/a \quad \text{(D.11)}$$

where c_i are coefficients to be determined. To obtain the solution for the same problem shown in Fig. 2-b, we substitute Eq. (D.11) into Eq. (D.5) and replace the stress field by P/x_o to obtain

$$K_I = P\sqrt{\pi a} \frac{f_0(a)}{x_o} \left\{ 1 - (1-x_o)^2(\frac{2}{\pi}) \cos^{-1} \left[\frac{x_o(1-a)}{a(1-x_o)} \right] [1 - \alpha \frac{x_o}{a}(1-a)(1 + \sum_{i=1}^{n} c_i a^i)] \right\} \quad \text{(D.12)}$$

Taking the limit of x approaching zero leads to

$$K_I = \frac{1.12P}{(1-a)^{3/2}}\sqrt{\frac{\pi}{a}}[\alpha + \frac{2}{\pi} + a(2-\alpha-\frac{2}{\pi}) + \alpha(1-a)\sum_{i=1}^{n} c_i a^i] \quad \text{(D.13)}$$

A comparison of Eq. (D.13) with Eq. (D.8) indicates that all higher order terms of a_i with $i > 1$ in Eq. (D.11) are redundant and coefficients c_i must vanish. Substituting Eqs. (D.3) and (D.7) into Eq. (D.4), the K_I solution may be expressed in a very compact form as

$$K_I = \frac{1.12\sqrt{\pi a}}{(1-a)^{3/2}}\int_0^a \frac{\partial}{\partial z}\left\{(1-(1-z)^2(\frac{2}{\pi})\cos^{-1}\left[\frac{z(1-a)}{(1-z)a}\right][1-\alpha z(1-a)/a]\right\}\sigma(z)dz \quad \text{(D.14)}$$

D.2 Results

Two loading conditions are considered. The first one is a parabolic stress distribution given by

$$\sigma(z) = \sigma_2(1-2z)^2 \quad \text{(D.15)}$$

The corresponding values of K_I have been obtained by Gregory [59] using an analytical solution. The second one is a linear stress distribution given by

$$\sigma(z) = \sigma_1(1-2z) \quad \text{(D.16)}$$

The values of K_I can also be obtained by using the weight functions given by Schindler [118] or by Fett and Munz [49].

Substituting Eqs. (D.15) and (D.16) into Eq. (D.14), the values of K_I/σ are computed and tabulated in Tables D.1 and D.2 respectively. The results obtained by Gregory and given by Schindler or Fett and Munz using weight function are also tabulated in the two tables. It is seen that the agreement with the analytical solution by Gregory is excellent and the agreement with the results by Schindler or Fett and Munz is also very good.

Table D.1. Comparison of Eq. (D.14) and exact solution [59] for a parabolic stress given by Eq. (D.15)

a/d	Eq.(D.14)	Ref.[59]	Eq. (14)/Ref. [59]
0.05	0.424592	0.425181	0.998614
0.10	0.577839	0.578924	0.998126
0.15	0.686358	0.688234	0.997274
0.20	0.776176	0.779163	0.996166
0.25	0.860120	0.864490	0.994944
0.30	0.947400	0.953339	0.993771
0.35	1.046424	1.053997	0.992815
0.40	1.166271	1.175407	0.992228
0.45	1.318009	1.328485	0.992115
0.50	1.516399	1.527838	0.992513
0.55	1.782608	1.794490	0.993379
0.60	2.149051	2.160730	0.994595
0.65	2.668774	2.679536	0.995983
0.70	3.435373	3.444533	0.997341
0.75	4.629964	4.637054	0.998471
0.80	6.648814	6.653977	0.999224
0.85	10.52746	10.53239	0.999532
0.90	19.88281	19.89363	0.999456
0.95	57.74163	57.78478	0.999253

Table D.2. Comparison of Eq. (D.14) with solutions [49] and [118] for a linear stress given by Eq. (D.16)

a/d	Eq.(D.14)	Ref. [118]	Ref.[49]
0.05	0.450909	0.45065	0.45078
0.10	0.650149	0.65084	0.65065
0.15	0.815304	0.81710	0.81646
0.20	0.968727	0.97218	0.97086
0.25	1.120928	1.12682	1.12443
0.30	1.279455	1.28879	1.28478
0.35	1.451465	1.46547	1.45905
0.40	1.645100	1.66523	1.65540
0.45	1.870766	1.89873	1.88417
0.50	2.142858	2.18062	2.15970
0.55	2.482530	2.53239	2.50303
0.60	2.922670	2.98730	2.94682
0.65	3.517533	3.60014	3.54488
0.70	4.363147	4.46769	4.39225
0.75	5.645298	5.77700	5.67239
0.80	7.769517	7.93599	7.78448
0.85	11.79163	12.0058	11.7643
0.90	21.38246	21.6732	21.1986
0.95	59.78601	60.2655	58.6965

E

Stress Variation With the Location of the Virtual Forces on a Disk

Consider a pair of opposite forces F acting along a vertical chord $\overline{AB}$ of a disk shown in Fig. E.1. Assuming that each of the forces produces a simple radial stress distribution[124], the normal stress σ'_y at location C along a horizontal line $\overline{MN}$ passing the center of the disk O is given by

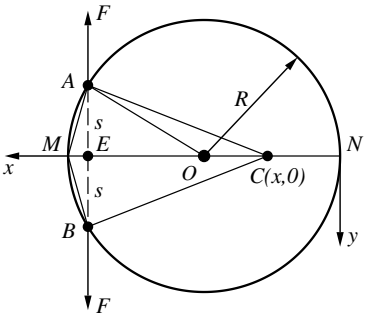

Fig. E.1. A disk of diameter $D = 2R$ subjected to a pair of forces F along chord $\overline{AB}$ of length $2s$.

$$\sigma'_y(x,0) = \frac{4F}{\pi s}(1-\cos^2\beta)\cos^2\beta \tag{E.1}$$

where s is the distance from F to $\overline{MN}$ and β is the angle between chord $\overline{AB}$ and the radius from F to location C. In rectangular coordinates with origin located at N, $\cos^2\beta$ in Eq. (E.1) is given as

$$\cos^2\beta = \frac{s^2}{R^2 + (R-s)^2 + 2(R-x)\sqrt{R^2 - s^2}} \tag{E.2}$$

where R is the radius of the disk and x is the distance from C to N. It is shown in [124] that Eq. (E.1) produces a uniform tension around the disk. For a stress-free boundary we need to superpose a uniform tension around the disk with an opposite sign, which is given by

$$\sigma = \frac{2F}{\pi D}\sin(\theta + \theta_1) \tag{E.3}$$

where θ and θ_1 are angles between chord $\overline{AB}$ and the distance from A or B to a location on the rim of the disk. Noticing $\theta + \theta_1$ is constant, we can write the corresponding normal stress on plane $\overline{MN}$ as

$$\sigma''_y(x,0) = \frac{4F}{\pi D}\sin\theta\cos\theta = \frac{4F}{\pi D}\frac{\overline{ME}\ \overline{AE}}{\overline{AM}^2} = \frac{4F}{\pi D}\frac{s}{2R} \tag{E.4}$$

where θ is the angle between $\overline{AB}$ and $\overline{AM}$ or $\overline{BM}$. Carrying out the partial differentiations with respect to F and s, and setting s to zero leads to[1].

$$\frac{\partial^2\sigma_y(x,0)}{\partial F\partial s}_{|s=0} = \frac{\partial^2\sigma'_y(x,0)}{\partial F\partial s}_{|s=0} + \frac{\partial^2\sigma''_y(x,0)}{\partial F\partial s}_{|s=0} = 0 + \frac{4P}{\pi D^2} \tag{E.5}$$

[1] The result of Eq. (E.5) was first obtained during the work of [39]

F

Nonuniform Strain Measured Over a Finite Length of an Electric Resistance Strain Gage

Electric resistance strain gages have been used in many applications because of their accuracy and convenience. However, in situations where the length of a strain gage is large compared with the size of a region with a rapidly varying strain gradient, a question arises whether the relation based on a uniform strain field is still valid. In this note we will show that the relation is still valid provided that the average strain over the length of the gage is used.

When a uniaxial load is applied to a conductor of length L_o and cross-section area $A_o = w_o t_o$, the change of the resistance may be related to the strain ϵ , Poisson's ratio ν and specific resistance p by [41]

$$\frac{dR}{R_o} = \epsilon(1 + 2\nu) + \frac{dp}{p} \tag{F.1}$$

assuming ϵ is small and uniform.

In what follows we will demonstrate that, if the strain varies along the length, Eq. (F.1) is still valid provided that ϵ is replaced by the average strain ϵ_m. Since the specific resistance is much less influenced by the dimensional change of the strain gage, we replace p by p_m, which is uniform along the length and only dependent on ϵ_m.

The expression for resistance is now given by

$$R = p_m \int_0^{L_0+\Delta L} \frac{ds}{A(s)} + dp\frac{L_0}{A_0} \tag{F.2}$$

in which s is the distance in the longitudinal direction. Assuming a rectangular cross section of width w and thickness t, the area A is given by

$$A = w \times t = A_0(1 + \frac{dw}{w_0})(1 + \frac{dt}{t_0}) = A_0[1 - 2\nu\epsilon(s) + \nu^2\epsilon^2(s)] \tag{F.3}$$

The change of resistance is thus given by

$$\frac{R - R_0}{R_0} = \int_0^{L_0+\Delta L} \frac{(ds/L_0)}{1 - 2\nu\epsilon(s) + \nu^2\epsilon^2(s)} - 1 + \frac{dp}{p_m}$$

$$= \int_0^{1+\epsilon_m} \frac{ds'}{1 - 2\nu\epsilon(s') + \nu^2\epsilon^2(s')} - 1 + \frac{dp}{p_m} \tag{F.4}$$

in which $s' = s/L_o$. To check Eq. (F.4), we let ϵ be a constant, i.e.,

$$\int_0^{1+\epsilon} \frac{ds'}{1 - 2\nu\epsilon + \nu^2\epsilon^2} - 1 = \frac{1+\epsilon}{1 - 2\nu\epsilon + \nu^2\epsilon^2} - 1$$
$$= \frac{\epsilon + 2\nu\epsilon - \nu^2\epsilon^2}{1 - 2\nu\epsilon + \nu^2\epsilon^2} \approx \epsilon(1 + 2\nu) \tag{F.5}$$

which, when substituted into Eq. (F.4), leads to an expression identical to Eq. (F.1).

Consider an n^{th} order nonuniform strain field which may take a form as

$$\epsilon_n(s') = \epsilon_m(n+1)(s')^n \tag{F.6}$$

where ϵ_m is the average strain of $\epsilon_n(s')$. Using Eq. (F.6), the first term in Eq. (F.4) becomes

$$\int_0^{1+\epsilon_m} \frac{ds'}{1 - 2\nu\epsilon_m(1+n)(s')^n + \nu^2\epsilon_m^2(1+n)^2(s')^{2n}} - 1 \tag{F.7}$$

As a comparison we tabulate the values of the ratio of Eq. (F.7) to the first term of Eq. (F.1) in Table F.1 for various values of ν, ϵ_m and n. It is seen that the difference varies slightly with different values of n and ν, and it is nearly proportional to ϵ_m. It should be pointed out that if any uniform strain is included in Eq. (F.6) the combined differences will be smaller than those tabulated in Table F.1. Thus, we may conclude that for elastic deformation Eq. (F.1) is sufficiently accurate to obtain the average strain over a region of nonuniform strain. In other words, the strain measured by an electrical-resistance strain gage represents closely the average strain over the length of the gage.

Table F.1. Ratio of Eq. (F.7) to Eq. (F.1) for different values of ϵ_m and ν for $n = 1$ to $n = 3$

$n = 1$	$\epsilon_m = 0.1$	$\epsilon_m = 0.01$	$\epsilon_m = 0.001$	$\epsilon_m = 0.0001$
ν =0.25	1.09347	1.00843	1.00083	1.00008
ν =0.30	1.11081	1.00987	1.00098	1.00010
ν =0.35	1.12084	1.01127	1.00111	1.00011
$n = 2$	$\epsilon_m = 0.1$	$\epsilon_m = 0.01$	$\epsilon_m = 0.001$	$\epsilon_m = 0.0001$
$\nu = 0.25$	1.15005	1.01248	1.00123	1.00012
$\nu = 0.30$	1.17872	1.01458	1.00143	1.00014
$\nu = 0.35$	1.20761	1.01661	1.00163	1.00016
$n = 3$	$\epsilon_m = 0.1$	$\epsilon_m = 0.01$	$\epsilon_m = 0.001$	$\epsilon_m = 0.0001$
$\nu = 0.25$	1.21831	1.01663	1.00161	1.00016
$\nu = 0.30$	1.26245	1.01941	1.00189	1.00019
$\nu = 0.35$	1.30780	1.02209	1.00215	1.00021

G

C++ Programs for the Calculation of Eq. (10.24)

Following the derivation of Eq. (A.5) we have

$$\int_0^a f(x,a)\left[\frac{S(\Delta s,1-x)}{\Delta s}\right]dx$$
$$=\int_0^1(1-va)(2a+G-3Gva)\cos^{-1}[\frac{(1-a)v}{1-av}]\frac{S(\Delta s,1-va)}{\Delta s}dv$$
$$+\int_0^{\pi/2}\frac{(1-a)^2[1-a+(a-G)\sin u]}{(1-a+a\sin u)^3}\frac{S(\Delta s,(1-a)/(1-a+a\sin u))}{\Delta s}du \quad \text{(G.1)}$$

The numerical integration of Eq. (G.1) is encapsulated in a C++ class, PointF. A sample C++ program is provided to show the usage of PointF. The program has been tested using the Microsoft® Visual studio.net C++ 2005.

G.1 PointF Class Header – Listing of PointF.h

```
#define GSQN 30 // number of Gaussian quadrature points
class PointF
{
public:
   PointF(void);
   ∼PointF(void);

// Gaussian-Lagrrier quadrature routine
   double infintg(double (PointF::*grand)(double));
// integrand for Gaussian-Lagrrier quadrature
   double integrandS(double x);
// Set gage length gl and offset dy for computing ave. strain
   void SetGPos(double x,double y) {gl=x; dy = y;};
   void SetNVal(int i);
```

```
// Compute stress due to F
   double FunS(double y);
//////////////////////////////////////////////////////
// A modified Gaussian quadrature
   double intek(double a, double b,double (PointF::*grand)(double));
   double Fun1(double v);
   double Fun2(double u);
   double FunF(double a);
private:
   int n; // number of Gaussian-Lagrrier quadrature points
   static double ab[GSQN];
   static double wb[GSQN];
   static double add[GSQN];
   static double wkb[GSQN];
   double (PointF::*f)(double x);
   double ao; // current normalized depth of cut
   double Ga; // current value of G(a)
   double yo; // normalized distance on cut plane for stress due to F
   double so; // distance from the position of F to the plane of cut
   double gl; // Gage length
   double dy; // Offset of gage center
};
```

G.2 Code for Class Definition – Listing of PointF.cpp

```
#include ‘‘pointf.h"
#define _USE_MATH_DEFINES
#include <math.h>

PointF::PointF(void)
:n(21), // accurate to at least 1.0e-9 for n = 21
ao(0), Ga(0) { }

PointF::~PointF(void) { }

//////////////////////////////////////////////////////
double PointF::ab[GSQN] =
{0.234526109519618537, 0.576884629301886424, 1.07244875381781771,
1.72240877644464545, 2.52833670642579507, 3.49221327302199439,
4.61645676974973095, 5.90395850417717807, 7.35812673158943653,
8.98294092506170375, 10.7830186325538887, 12.7636979795992374,
14.9311397434474381, 17.2924543449313719, 19.8558608677867421,
22.6308889326376814, 25.6286360941471892, 28.8621018735170335,
32.3466291442543635, 36.1004948095275791, 40.1457197693999658,
44.5092079943361867, 49.2243949878495185, 54.3337213335559171,
59.8925091630914400, 65.9753772877550561, 72.6876280911816123,
```

```
80.1874469777939813, 88.735340417914390, 98.8295428682851138};
double PointF::wb[GSQN] =
{0.21044310793881323, 0.23521322966984802, 0.19590333597288113,
0.12998378628607033, 0.070578623865717035, 0.031760912509175152,
0.011918214834847041, 0.0037388162946272654, 9.8080331147953040e-4,
2.1486491849068858e-4, 3.9203419695654058e-5, 5.9345416585029408e-6,
7.4164047196725324e-7, 7.6045677945004026e-8, 6.3506043286326967e-9,
4.2813811668291118e-10, 2.3058991426852954e-11, 9.7993789867899799e-13,
3.2378020233599416e-14, 8.1718229928234848e-16, 1.5421338096502519e-17,
2.1197923331866732e-19, 2.0544296755444497e-21, 1.3469825912970385e-23,
5.6612941065144460e-26, 1.4185605452783491e-28, 1.9133754915490041e-31,
1.1922487604782053e-34, 2.6715112191015198e-38, 1.3386169421024840e-42};
/* A Gaussian-Laguerre quadrature based on 32 nodes. Only the first
n nodes and corresponding weights are used in the program. User
can change the number of nodes used in the program by specifying
the value of computation n. */
double PointF::infintg(double (PointF::*grand)(double))
{
   int i;
   double vk,*pa,*pw;

   pa = ab;
   pw = wb;
   vk = (this->*grand)(0.044489365833267)*0.109218341952385;
   for(i=1;i<=n;++i)
      vk += (this->*grand)(*pa++)**pw++;
   return vk;
}
void PointF::SetNVal(int i)
{
   if(i>30)
      n = 30;
   else
      n = i;
}

double PointF::FunS(double y)
{
   double t,x,S1,S2;
   yo = y;
   x = 1.0-yo;
   so = gl/2.0+dy; // distance from centerline
   t = so*so+x*x;
   f = &PointF::integrandS;
   S1 = infintg(f)/so+4.0*so*so/(t*t);

   so = gl/2.0-dy; // distance from centerline
   t = so*so+x*x;
   f = &PointF::integrandS;
```

```
   S2 = infintg(f)/so+4.0*so*so/(t*t);
   return S1+S2;
}
// The integrand for stress due to horizontal point forces on lower edge
double PointF::integrandS(double x)
{
   double sh,chy,shy,xy,xy1,shy1,chy1,t1,t2,t3,t4;
   xy = x*(1.0-yo);
   sh = sinh(x);
   chy = cosh(xy);
   shy = sinh(xy);
   xy1 = x*yo;
   shy1 = sinh(xy1);
   chy1 = cosh(xy1);
// G(a,1-x)
   t1 = (xy1*shy-2*chy1+xy*shy1-2*chy)/(sh+x);
   t2 = (xy1*shy+2*chy1-xy*shy1-2*chy)/(sh-x);
   t1 = (x-1)*(t1+t2);
// H(a,1-x)
   t3 = (xy1*chy-shy1+xy*chy1-shy)/(sh+x);
   t4 = (xy1*chy+shy1-xy*chy1-shy)/(sh-x);
   t3 = x*(t3+t4);
   return (t1+t3)*sin(so*x);
}
//////////////////////////////////////////////////////////
double PointF::add[GSQN] =
{3.8220118431826414e-4, 2.0127000924398829e-3, 4.9416273837414745e-3,
9.1619943579814602e-3, 1.4662870583408546e-2, 2.1429924043507954e-2,
2.9445506659319426e-2, 3.8688709308522369e-2, 4.9135418762999415e-2,
6.0758381392559484e-2, 7.3527274576168277e-2, 8.7408785945670025e-2,
1.0236670035882018e-1, 1.1836199441384390e-1, 1.3535293827527645e-1,
1.5329520455275442e-1, 1.7214198395246456e-1, 1.9184410740103914e-1,
2.1235017432458469e-1, 2.3360668674853737e-1, 2.5555818886887394e-1,
2.7814741173073420e-1, 3.0131542263712170e-1, 3.2500177889796658e-1,
3.4914468551848464e-1, 3.7368115641547325e-1, 3.9854717874097075e-1,
4.2367787988459235e-1, 4.4900769671886297e-1, 4.7447054664601283e-1};
double PointF::wkb[GSQN] =
{9.8072668083514134e-4, 2.2804620030062086e-3,3.5761774958745448e-3,
4.8627309151780669e-3, 6.1366317539060523e-3, 7.3945329424689573e-3,
8.6331464938068718e-3, 9.8492388730505907e-3, 1.1039636574159522e-2,
1.2201233593772101e-2, 1.3330999262075445e-2, 1.4425986044091701e-2,
1.5483337184198697e-2, 1.6500294137953705e-2, 1.7474203758266676e-2,
1.8402525211577409e-2, 1.9282836603504086e-2, 2.0112841295499124e-2,
2.0890373895444246e-2, 2.1613405906248049e-2, 2.2280051017541744e-2,
2.2888570026572980e-2, 2.3437375375404533e-2, 2.3925035292547804e-2,
2.4350277528205763e-2, 2.4711992673367795e-2, 2.5009237054089127e-2,
2.5241235193398702e-2, 2.5407381834409172e-2, 2.5507243519348632e-2};
/* A Legendre-Gaussian quadrature using 41 nodes which is exact for
a polynomial of up to order 59 */
```

```
double PointF::intek(double ak,double bk,double(PointF::*grand)(double))
{
   int i;
   double sk,vk,ad,*pa,*pw;
   sk = bk - ak;
   vk = 0.025540559720393109*(this->*grand)(ak+.5*sk);
   pa = add;
   pw = wkb;
   for(i=1;i<=GSQN;++i)
   {
      ad = sk**pa++;
      vk += ((this->*grand)(ak+ad)+(this->*grand)(bk-ad))**pw++;
   }
   return vk*sk;
}
// Integrand for the first part of the integral defined in [0,1]
double PointF::Fun1(double v)
{
   double t1,t2;
   t1 = v*(1.0-ao)/(1-ao*v);
   t2 = (1.0-ao*v)*(2.0*ao+Ga-3.0*Ga*v*ao);
   return t2*acos(t1)*FunS(ao*v);
}
// Integrand for the second part of the integral defined in [0,π/2]
double PointF::Fun2(double u)
{
   double su,t1,t2,t3;
   su = sin(u);
   t1 = 1.0-ao;
   t2 = t1+ao*su;
   t3 = t1*t1*(t1+(ao-Ga)*su)/(t2*t2*t2);
   return t3*FunS(ao*su/t2);
}
// Compute the integral for a given value of a
double PointF::FunF(double a)
{
   ao = a; // store the value of normalized crack size
   Ga = 3.0*(1.0-7.0*ao)*pow(1.0-ao,5.0)/28.0;
   double f1,f2;
   f = &PointF::Fun1;
   f1 = intek(0.0,1.0,f);
   f = &PointF::Fun2;
   f2 = intek(0.0,M_PI_2,f);
   return (f1+f2)/M_PI_2;
}
```

G.3 Sample Code for Usage of Class PointF

```
#include ‘‘stdafx.h"
#include <iostream>
#include <fstream>
#include <string>
#include <iomanip>
#include ‘‘PointF.h"
int _tmain(int argc, _TCHAR* argv[])
{
   using namespace std;
   string str;
   size_t i,m;
   double x,x1,x2,y;
   double gl,dy;
   double thk;
// Create the class
   PointF Kf;

   cout << ‘‘Output file name: ";
   cin >> str;
   ofstream ofile(str.c_str());
   if(!ofile)
   {
      cerr << ‘‘Can’t open input file ‘‘" << str << "" " << endl;
      exit(EXIT_FAILURE);
   }
   cout << ‘‘Number of data to be computed = ";
   cin >> m;
   cout << ‘‘Starting and ending points on plane of cut = ";
   cin >> x1 >> x2;
   cout << ‘‘Thickness = ";
   cin >> thk;
   cout << ‘‘Gage length = ";
   cin >> gl;
   cout << ‘‘Gage position offset = ";
   cin >> dy;
   if(dy>=gl/2)
   {
      cout << ‘‘Error: Strain gage is off the centerline." << endl;
      exit(EXIT_FAILURE);
   }
// Compute the values of f^f(a,s)
   Kf.SetGPos(gl/thk,dy/thk);
   for(i=0;i<=m;i++)
   {
      x = (x1+(x2-x1)*i/m)/thk;
      y = Kf.FunF(x);
```

```
      ofile << std::fixed << x << '\t' << std::scientific
            << std::setprecision(10) << y << endl;
   }
   cout << ``Completed." << endl;
   return 0;
}
```

References

1. K. E. Atkinson. An Intorduction to Numerical Analysis. John Wiley and Sons, New York, Chichester, Brisbane, Toronto, 1978.
2. C. C. Aydiner, E.Üstündag, M. B. Prime, and A. Peker. Modeling and measurement of residual stresses in bulk metallic glass plate. *Journal of Non-Crystalline Solids*, 316:82–95, 2003.
3. C. C. Aydiner and E. Üstündag. Residual stresses in a bulk metallic glass cylinder induced by thermal tempering. *Mechanics of Materials*, 37:201–212, 2004.
4. J. Lu A. Niku-Lari and J. F. Flavenot. Measurement of residual-stress distribution by the incremental hole-drilling method. *Experimental Mechanics*, 25:175–185, 1985.
5. N. P. Bansal and R. H. Doremus. *Handbook of Glass Properties*. Academic, Orlando, Florida, USA, 1986.
6. E. M. Beaney. Accurate measurement of residual stress on any steel using the centre hole method. *Strain*, 12:99, 1976.
7. M. Bijak-Zochowski. A semidestructive method of measuring residual stresses. *VID-Berichte*, 313:469–476, 1978.
8. E. Brinksmeier, J. T. Cammett, P. Leskovar W. Knig, J. Peters, and H. K. Tnshoff. Residual stresses - measurement and causes in machining processes. *Annals of CIRP*, 31:491–510, 1982.
9. H. F. Bueckner. Field singularity and integral expressions. In G. C. Sih, editor, *Methods of Analysis and Solutions of Crack Problems*, chapter 5, page 239. Noordhoff International publishing, Groningen, 1973.
10. G. Chell. The stress intensity factor for center and edge cracked sheets subjected to an arbitrary loading. *Fracture Mechanics*, 7:137–152, 1975.
11. Weili Cheng and Iain Finnie. A method for measurement of axisymmetric residual stresses in circumferentially welded thin-walled cylinders. *ASME Journal of Engineering Materials and Technology*, 106:181–185, 1985.
12. Weili Cheng and Iain Finnie. On the prediction of stress intensity factors for axisymmetric cracks in thin-walled cylinders from plane strain solutions. *ASME Journal of Engineering Materials and Technology*, 106:227–231, 1985.
13. Weili Cheng and Iain Finnie. Determination of stress intensity factors for partial penetration axial cracks in thin-walled cylinders. *ASME Journal of Engineering Materials and Technology*, 108:83–86, 1986.

14. Weili Cheng and Iain Finnie. Examination of the computational model of the layer removal method. *Experimental Mechanics*, 26:150–153, 1986.
15. Weili Cheng and Iain Finnie. Measurement of residual hoop stresses in cylinders using the compliance method. *ASME Journal of Engineering Materials and Technology*, 108:87–92, 1986.
16. Weili Cheng and Iain Finnie. A new method for measurement of residual axial stresses applied to a multi-pass butt-welded cylinder. *ASME Journal of Engineering Materials and Technology*, 109:337–342, 1987.
17. Weili Cheng and Iain Finnie. K_I solutions for an edge-cracked strip. *Eng. Fracture Mech.*, 31:201–207, 1988.
18. Weili Cheng and Iain Finnie. Stress intensity factors for radial cracks in cylinders and other simply closed bodies. *Eng. Fracture Mechanics*, 362:767–774, 1989.
19. Weili Cheng and Iain Finnie. The crack compliance method for residual stress measurement. *Welding in the World*, 28:103–110, 1990.
20. Weili Cheng and Iain Finnie. A K_{II} solution for an edge-cracked strip. *Eng. Fracture Mechanics*, 36:355–360, 1990.
21. Weili Cheng and Iain Finnie. An experimental method for determining residual stresses in welds. In M. Rappaz, editor, *Modeling of Casting, Welding and Advanced Solidification Processes - V*. The Minerals Metals and Materials Soc., 1991.
22. Weili Cheng and Iain Finnie. Measurement of residual stress distributions near the toe of a weld between a bracket and a plate using the crack compliance method. In L. Karisson, L. Lindgren, and M. Jonsson, editors, *Proc. of IUTAM Symposium, Mechanical Effects of Welding*, pages 135–141, Berlin Heidelberg, 1992. Springer-Verlag.
23. Weili Cheng and Iain Finnie. A prediction on the strength of glass following the formation of subsurface flaws by scribing. *J. of the American Ceramic Society*, 75:2565=–2572, 1992.
24. Weili Cheng and Iain Finnie. A comparison of the strains due to edge cracks and cuts of finite width with applications to residual stress measurement. *ASME Journal of Engineering Materials and Technology*, 115:220–226, 1993.
25. Weili Cheng and Iain Finnie. Measurement of residual stress distributions near the toe of an attachment welded to a plate using the crack compliance method. *Eng. Fracture Mechanics*, 46:79–92, 1993.
26. Weili Cheng and Iain Finnie. An overview of the crack compliance method for residual stress measurement. In *Proceedings of the Fourth International Conference on Residual Stresses*, pages 449–458, Baltimore, 1994.
27. Weili Cheng and Iain Finnie. Computation of stress intensity factors for a 2-d body from displacements at an arbitrary location. *Int. J. of Fracture*, 81:259–267, 1996.
28. Weili Cheng and Iain Finnie. Residual stress measurement by the introduction of slots or cracks. In Nisitani et al, editor, *Localized Damage IV*, pages 37–51. Computation Mechanics Publications, 1996.
29. Weili Cheng and Iain Finnie. The single-slice method for measurement of axisymmetric residual stresses in solid rods or hollow cylinders in the region of plane strain. *ASME Journal of Engineering Materials and Technology*, 120:170–176, 1998.

30. Weili Cheng. Measurement of the axial residual stresses using the initial strain approach. *ASME Journal of Engineering Materials and Technology*, 122:135–140, 2000.
31. W. Cheng, I. Finnie, M. Gremaud, A. Rosselet, and R.D. Streit. The compliance method for measurement of near surface residual stresses - application and validation for surface treatment by laser and shot-peening. *ASME Journal of Engineering Materials and Technology*, 116:556–560, 1994.
32. W. Cheng, I. Finnie, and Mike B. Prime. Measurement of residual stresses through the thickness of a strip using the crack-compliance method. In H. Fujiwara, T. Abe, and K. Tanaka, editors, *Residual Stresses - III Science and Technology*, pages 1127–1132, London and New York, 1992. Elsevier Science Publishers.
33. W. Cheng, I. Finnie, and R. O. Ritchie. Residual stress measurement on pyrolytic carbon-coated graphite leaflets for cardiac valve prostheses. In *Proc. 2001 SEM Annual Conference on Experimental and Applied Mechanics*, pages 604–607. Portland, Oregon, June 2001.
34. W. Cheng, I. Finnie, and Ö. Vardar. Measurement of residual stresses near the surface using the crack compliance method. *ASME Journal of Engineering Materials and Technology*, 113:199–204, 1990.
35. W. Cheng, I. Finnie, and Ö. Vardar. Deformation of an edge-cracked strip subjected to arbitrary shear surface traction on the crack faces. *Eng. Fracture Mechanics*, 43:33–40, 1992.
36. W. Cheng, I. Finnie, and Ö. Vardar. Deformation of an edge cracked strip subjected to normal surface traction on the crack faces. *Eng. Fracture Mech.*, 42:97–108, 1992.
37. W. Cheng, I. Finnie, and Ö. Vardar. Estimation of axisymmetric residual stresses in a long cylinder. *ASME Journal of Engineering Materials and Technology*, 114:137–140, 1992.
38. W. Cheng, M. Gremaud, M. Prime, and I. Finnie. Measurement of near surface residual stress using electric discharge wire machining. *ASME Journal of Engineering Materials and Technology*, 116:1–7, 1994.
39. W. Cheng, H. J. Schindler, and I. Finnie. Measurement of residual stress distribution in a disk or solid cylinder using the crack compliance technique. In *Proceedings of the Fourth International Conference on Residual Stresses*, Baltimore, 1994.
40. W. Cheng, G. Stevick, and I. Finnie. Prediction of the stress intensity factor for an internal circumferential crack at a butt-weld between cylinders using plane strain solutions. *ASME Journal of Engineering Materials and Technology*, 106:21–24, 1984.
41. J. W. Dally and W. F. Riley. *Experimental Stress Analysis*. MacGraw-Hill, Inc, N. Y.
42. Adrian T. DeWald and Michael R. Hill. Improved data reduction for the deep hole method of residual stress measurement. *J. of Strain Analysis for Engineering Design*, 38:65–78, 2003.
43. A.T. Dewald, J.E. Rankin, M.R. Hill, and K.I. Schaffers. An improved cutting plan for removing laser amplifier slabs from yb:s-fap single crystals using residual stress measurement and finite element modeling. *Journal of Crystal Growth*, 265:627–641, 2004.

44. A. T. DeWald, J. E. Rankin, M. R. Hill, M. J. Lee, and H. L. Chen. Assessment of tensile residual stress mitigation in alloy 22 welds due to laser peening. *ASME Journal of Engineering Materials and Technology*, 126:465–473, 2004.
45. R. R. de Swardt. Finite element simulation of crack compliance experiments to measure residual stresses in thick-walled cylinders. *J. Pressure Vessel Tech.*, 125:305–308, 2003.
46. C. Dalle Donne, G. Biallas, T. Ghidini, and G. Raimbeaux. Effect of weld imperfections and residual stresses on the fatigue crack propagation in friction stir welded joints. In *Proc. 2nd Int. Conf on Friction Stir Welding*, pages 26–28. Gothenberg Sweden, June 2000.
47. F. M. Ernsberger. Detection of strength-impairing surface flaws in glass. *Proc. Royal Soc.*, 257A:213–223, 1960.
48. N. Ersoy and Ö. Vardar. Measurement of residual stresses in layered composites by compliance method. *J. Composite Materials*, 34:575–598, 2000.
49. T. Fett and D. Munz. Proceedings 23, Vortragsveranstaltung des DVM-Arbetskreises Bruchvorgnge. Berlin, pages 249–259, 1991.
50. T. Fett. Bestimmung von eigenspannungen mittels bruchmechanischer beziehungen (determination of residual stresses by use of fracture mechanical relations). *Materialprfung*, 29:92–92, 1987.
51. Iain Finnie and Weili Cheng. Residual stresses and fracture mechanics. *ASME Journal of Engineering Materials and Technology*, 117:373–378, 1995.
52. Iain Finnie and Weili Cheng. A summary of past contributions on residual stresses. In *ECRS6* 6^{th} *European Conf. on Residual Stresses*, pages 509–514, Coimbra, Portugal, 2002.
53. I. Finnie, W. Cheng, and K. J. McCorkindale. Delayed crack propagation in a steel pressure vessel due to thermal stresses. *Int. J. Pres. Ves. and Piping*, 42:15–31, 1990.
54. S. Finnie, W. Cheng, and I. Finnie. The computation and measurement of residual stresses in laser deposited layers. *ASME Journal of Engineering Materials and Technology*, 125:1–7, 2003.
55. M.T. Flaman. Brief investigation of induced drilling stresses in the center-hole method of residual-stress measurement. *Experimental Mechanics*, 1982.
56. Y. C. Fung. *Foundations of Solid Mechanics*. Prentice-Hall, Englewood Cliffs, N.J., 1965.
57. J.M. Ganley, A. K. Maji, and S. Huybrechts. Explaining spring-in in filament wound carbon fiber/epoxy composites. *J. Composite Materials*, 34:1216–1239, 2000.
58. C. J. Gilbert, V. Schroeder, and R. O. Ritchie. Mechanisms for fracture and fatigue-crack propagation in a bulk metallic glass. *Metall. & Mater. Trans. A*, 30:1739–1754, 1999.
59. R. D. Gregory. The spinning circular disc with a radial edge crack; an exact solution. *Int. J. of Fracture*, 41:39–50, 1989.
60. M. Gremaud, W. Cheng, I. Finnie, and M.B. Prime. The compliance method for measurement of near surface residual stresses - analytical background. *ASME Journal of Engineering Materials and Technology*, 116:550–555, 1994.
61. A. A. Griffith. The phenomena of rupture and flow in solids. *Phil Trans.*, 221A:163–198, 1921.
62. J. P. Den Hartog. *Advanced Strength of Materials*. McGraw-Hill, New York, 1952.

63. R. J. Hartrenft and G. G. Sih. Alternating method applied to edge and surface crack problems. In G. C. Sih, editor, *Methods of Analysis and Solutions of Crack Problems*, chapter 5, page 179. Noordhoff International publishing, 1973.
64. E Heyn and O. Bauer. ber spannungen in kaltgereckten metallen. *Int. Z. f. Metallographie*, 1:16, 1910.
65. Michael R. Hill and Wei-Yan Lin. Residual stress measurement in a ceramic-metallic graded material. *ASME Journal of Engineering Materials and Technology*, 124:185–191, 2001.
66. M. R. Hill and D. V. Nelson. Determining residual stress through the thickness of a welded plate. *ASME J. of PVP*, 318:343–352, 1996.
67. M. R. Hill and D. V. Nelson. Determining residual stress through the thickness of a welded plate. *ASME J. of PVP*, 327:29–36, 1997.
68. M. R. Hill and D. V. Nelson. The localized eigenstrain method for determination of triaxial residual stress in welds. *ASME J. of PVP*, 373:397–403, 1998.
69. G. R. Irwin. Fracture. In S. Flugge, editor, *Encycl. of Physics*, volume VI. Springer-Verlag, 1958.
70. D. E. Johnson and J. R. Johnson. *Mathematical Methods in Engineering and Physics.* Prentice-Hall, Inc, Englewood Cliffs, N. J., 1982.
71. M.R. Johnson, R.R. Robinson, A.J. Opinsky, M.W. Joerms, and D.H. Stone. Calculation of residual stresses in wheels from saw cut displacement data. Technical Report 85-WA/RT-16, 1985.
72. K.J. Kang, J.H. Song, and Y.Y. Earmme. A method for the measurement of residual stresses using a fracture mechanics approach. *Journal of Strain Analysis*, 24:23–30, 1989.
73. K. J. Kang, S. Darzens, and G. S. Choi. Effect of geometry and materials on residual stress measurement in thin films by using the focused ion beam. *ASME Journal of Engineering Materials and Technology*, 126:457–464, 2004.
74. D. A. Lados and D. Apelian. The effect of residual stress on the fatigue crack growth behavior of al-si-mg cast alloys - mechanisms and corrective mathematical models. *Metallurgical and Materials Transactions A*, 37A:133–145, 2006.
75. W. K. Lim, J. H. Song, , and Sankar B. V. Effect of ring indentation on fatigue crack growth in an aluminum plate. *Int. Journal of Fatigue*, 25:1271–1277, 2003.
76. J. Lu, editor. *Handbook of measurement of residual stresses.* Society for Experimental Mechanics, Lilburn, GA, 1996.
77. K. Masubushi. *Analysis of Welded Structures.* Pergamon Press, 1980.
78. J. Mathar. Determination of initial stresses by measuring the deformation around drilled holes. *Trans., ASME,* Iron Steel, 56(2):249–254, 1934.
79. R. Mayville and I. Finnie. Uniaxial stress-strain curves from a bending test. *Experimental Mechanics*, 22:197, 1982.
80. F. A. McClintock and A. S. Argon. *Mechanical Behavior of Materials.* Addision-Wesley, Reading, MA, 1966.
81. Measurement Group, Inc., Raleigh, NC. *Measurement of Residual Stresses by The Hole-Drilling Strain-Gage Method*, tech note tn503-2 edition, 1986.
82. M. Mesnager. Methode de determination des tensions existant dans un cylindre circulaire. *Academie des Sciences*, 169:1391, 1919.
83. C. R. Morin, R. J. Shipley, and J. A. Wilkinson. Fractography, nde, and fracture mechanics applications in failure studies. *Materials Characterization*, 33, 1994.

84. R. E. Mould. The strength and static fatigue of glass. *Glasstechn. Ber.*, III:18–28, 1959.
85. R. L. Martineau M. B. Prime. Mapping residual stresses after foreign object damage using the contour method. *Materials Science Forum*, 404-407:521–526, 2002.
86. H. Nisitani. Two-dimensional problem solved using a digital computer, 1967.
87. H. Nisitani. Solutions of notch problems by body force method. In G. C. Sih, editor, *Stress Analysis of Notch Problems, in Mechanics of Fracture*, 1978.
88. D. Nowell, S. Tochilin, and D. A. Hills. Use of the crack compliance method for the measurement of residual stress. In *Proc. of the 6th Int. Conf. on Residual Stresses*, volume 2, pages 845–852. Oxford, U.K., July 2000.
89. D. Nowell. Strain changes caused by finite width slots, with particular reference to residual stress measurement. *J. Strain Anal. Eng. Des.*, 34:285–294, 1999.
90. I. C. Noyan and J. B. Cohen. *Residual Stress Measurement by Diffraction and Interpretation.* MRE. New York, 1987.
91. R. Pathania, W. Cheng, M. Kreider, N. Cofie, and J. Brihmadesam. Analytical and experimental evaluation of residual stresses in bwr core shroud welds. In *ASME Press. Vess. and Piping Division Pub.*, volume PVP 373, pages 337–349. 1998.
92. H. J. Petroski and J. D. Achenbach. Computation of the weight function from a stress intensity factor. *Eng. Fracture Mechanics*, 10:257–266, 1978.
93. W. D. Pilkey. *Formulas for stress, strain and structural matrices.* Wiley, New York, 1994.
94. P. S. Prevey. Problems with non-destructive surface x-ray diffractiuon reisdual stress measurement. In C. Ruud, editor, *ASM Conf. Pro., Practical Applications of Residual Stress Technology*, pages 47–54, 1991.
95. M.B. Prime and I. Finnie. Surface strains due to face loading of a slot in a layered half-space. *ASME Journal of Engineering Materials and Technology*, 118:410–418, 1996.
96. M.B. Prime and Ch. Hellwig. Residual stresses in a bi-material laser clad measured using compliance. In T. Ericsson et al., editor, *The Fifth International Conference on Residual Stresses*, pages 127–132, Sweden, 1997. Linkping University.
97. M.B. Prime and M.R. Hill. Measurement of fiber-scale residual stress variation in a metal-matrix composite. *Journal of Composite Materials*, 38:2079–2095, 2004.
98. Mike B. Prime. Residual stress measurement by successive extension of a slot: The crack compliance method. *Applied Mechanics Reviews*, 52:75–96, 1999.
99. Mike B. Prime. Cross-sectional mapping of residual stresses by measuring the surface contour after a cut. *ASME Journal of Engineering Materials and Technology*, 123:162–168, 2001.
100. M. B. Prime and M. R. Hill. Uncertainty, model error, and order selection for series-expanded, residual-stress inverse solutions. *ASME Journal of Engineering Materials and Technology*, 128:175–185, 2006.
101. M. B. Prime. Experimental verification of the crack compliance method. M.s. project report, University of California, Berkeley, 1991.
102. E. Procter and B.M. Beaney. The trepan or ring-core method, centre-hole methods, sach's method and blind hole methods and deep hole technique. In *Advances in Surface Treament Technology, Vol. 4, Residual Stresses*, page 165. Permagon Press, New York, 1987.

103. I. S. Raju and Jr. J. C. Newman. Stress-intensity factors for a wide range of semi-elliptical surface cracks in finite-thickness plates. *Eng. Fracture Mechanics*, 11:817–829.
104. Jon E. Rankin, Michael R. Hill, and Lloyd A. Hackel. The effects of process variations on residual stress in laser peened 7049 t73 aluminum alloy. *Materials Science and Engineering A*, 349:279–291, 2003.
105. Jon E. Rankin and Michael R. Hill. Measurement of thickness-average residual stress near the edge of a thin laser peened strip. *ASME Journal of Engineering Materials and Technology*, 125:283–293, 2003.
106. C.N. Reid. A method of mapping residual stress in a compact tension specimen. *Scripta Metallurgica*, 22:451–456, 1988.
107. N. J. Rendler and I. Vigness. Hole-drilling strain gage method of measuring residual stresses. *Experimental Mechanics*, 6:577–586, 1966.
108. J. R. Rice. Some remarks on elastic crack-tip stress fields. *Int. J. Solid Structures*, 8:751–758, 1972.
109. D. Ritchie and R.H. Leggatt. The measurement of the distribution of residual stress through the thickness of a welded joint. *Strain*, pages 61–70, May 1987.
110. R. O. Ritchie. 1996.
111. D. P. Rooke and D. J. Cartwright. *Compendium of Stress Intensity Factors*. H.M.S.O., London, 1976.
112. E. F. Rybicki, J. R. Shadley, and W. S. Shealy. A consistent-splitting method for experimental residual-stress analysis. *Exp. Mech.*, 23:438–445, 1983.
113. G. Sachs. Der nachweis innerer spannungen in stangen und rohren. *Zeits Zeitshrift fr Metalkunde*, 19:352, 1927.
114. G. S. Schajer. Measurement of non-uniform residual stresses using the hole-drilling method. part *I*-stress calculation procedures. *ASME Journal of Engineering Materials and Technology*, 1103:338–343, 1988.
115. G. S. Schajer. Measurement of non-uniform residual stresses using the hole-drilling method. part ii-practical application of the integral method. *ASME Journal of Eng. Mat. and Tech.*, 110:344–349, 1988.
116. H.J. Schindler. Determination of residual-stress distributions from measured stress intensity factors. *Int. J. of Fracture*, 74:R23–R30, 1996.
117. H. J. Schindler, W. Cheng, and I. Finnie. Experimental determination of stress intensity factors due to residual stresses. *Experimental Mechanics*, 37:272–277, 1997.
118. H. J. Schindler. Weight functions for deep cracks and high stress gradients. In *ICF8*, Kiev, 1993.
119. H. J. Schindler. Residual stress measurement in cracked components: Capabilities and limitations of the cut compliance method. *Materials Science Forum*, 347-349:150–155, 2000.
120. G. S. Schjaer. Application of finite element calculation to residual stress measurements. *ASME Journal of Eng. Mat. and Tech.*, 1981.
121. W. Soete and R. Vancrombrugge. An industrial method for the determination of residual stresses. *Proceedings, SESA*, 8:17, 1950.
122. F. Stablein. Spannungsmessungen in eiseiting abgeloschten knüppeln. *Monatshefte*, 12:93–99, 1931.
123. H. Tada, P. Paris, and G. Irwin. *The Stress Analysis of Cracks Handbook*. Del Research Corperation, PA, 1973.
124. S. P. Timoshenko and J. N. Goodier. *Theory of Elasticity*. McGraw-Hill, New York, 1952.

125. S. Tochilin, D. Nowell, and D. A. Hills. Residual stress measurement by the crack compliance technique. In *Proc. 11th Int. Conf. on Exp. Mech.*, volume 2, pages 1313–1318. Oxford, UK, 1998.
126. R. G. Treuting and W. T. Read Jr. A mechanical determination of biaxial residual stress in sheet materials. *J. Appl. Phys.*, 22:131, 1951.
127. Murakawa H. Ueda, Y. and N. X. Ma. Measuring method for residual stresses in explosively clad plates and a method of residual stress reduction. *ASME Journal of Engineering Materials and Technology*, 118:576–582, 1996.
128. Y. Ueda, K. Fukuda, and Y. C. Kim. New measuring method of axisymmetric three-dimensional residual stresses using inherent strains as parameters. *ASME Journal of Engineering Materials and Technology*, 108:328–334, 1986.
129. Y. Ueda and K. Fukuda. New measuring method of three-dimensional residual stresses in long welded joints using inherent strains as parameters - lz method. *ASME Journal of Engineering Materials and Technology*, 111, 1989.
130. S. Vaidyanathan and I. Finnie. Determination of residual stresses from stress intensity factor measurements. *Journal of Basic Engineering*, 93:243–246, 1971.
131. S. M. Wiederhorn, H. Johnson, A. M. Diness, and A. H. Heuer. Fracture of glass in vacuum. *J. Am. Ceram. Soc.*, 57:336–341, 1974.
132. X. R. Wu and A. J. Carlsson. Weight functions and stress intensity factor solutions. 1991.
133. O. C. Zienkiewicz. *The Finite Element Method*. McGraw-Hill Book Company Limited, 3rd edition.
134. *E837-89 Standard Test Method for Determining Residual Stresses by the Hole-Drilling Strain-Gage Method*, 1989.

Index

E, *see* elastic modulus
E' for plane stress or plane strain, 34
J-integral, 54
$J_n(x)$, Jacobi polynomials of n^{th} order, 13
K_I for an edge-cracked disk, 180
$K_I(a)$, Mode I stress intensity factor for a general normal stress, 34
$K_I^f(a)$, Mode I stress intensity factor for a horizontal line force F, 34
$K_I^q(a)$, Mode I stress intensity factor for a vertical line force Q, 34
$K_{II}(a)$, Mode II stress intensity factor for a general shear stress, 40
$K_{II}^h(a)$, Mode II stress intensity factor for a horizontal line force Q_h, 40
$K_{II}^v(a)$, Mode II stress intensity factor for a vertical line force Q_v, 40
$L_i(x)$, Legendre polynomial of i^{th} order, 12
T_i Chebyshev polynomial of i^{th} order, 76
U strain energy, 34
Δ_p, error bound on the peak variation, 111
Δ_{n+1},overall deviation, 107
δ_i, main deviation, 106
ϵ normal strain, 24
ϵ_m, average strain, 185
η, combined error bound, 112
η_e, error bound based on oscillation of the estimated stresses, 112
η_l, error that resembles a strain variation produced by an unbalanced load, 113, 114
ν, *see* Poisson's ratio
σ normal stress, 11, 20, 39
τ shear stress, 12, 20, 40
ζ, exponent of weight, 81
a, for
  depth of crack, 33
  depth of cut, 9
  thickness of a slice, 124
$cond([\overline{\boldsymbol{C}}])$, condition of compliance matrix, 77
$w(a_k/t)$, the weight applied to the k^{th}, depth, 81
$[\boldsymbol{C}]$, compliance matrix, 74

alignment of cutting path, 104
amplitude factor, 39, 73
annular element, 45
approximation
  initial strain, 137
  power series, 72
  used for unknown stress, 69
array of gages, 31
asymmetric geometry, 59
average strain, 98, 160
average strain due to
  linear stress, 26
  quadratic stress, 26
  uniform stress, 26
averaged estimates, 107
axial crack, 33
axisymmetric axial residual stress, 45

axisymmetric residual stresses, 117

beam subjected to bending, 103
BFM, *see* body force method
body force method, 19
boring-out method, 5
Bueckner's principle, 9

cardiac devices, 146
Castigliano's theorem, 33, 40, 42
change of strain energy, 156
Chebyshev polynomial, 58, 169
Chebyshev polynomial, 4^{th} order, 93
Chebyshev series, 79
choice of slice thickness, 129
clamping force, 18
closing of crack mouth, 164
combined error, 114
comparison
  a slot and a crack, 25
  avergae strain due to normal and shear stresses, 61
  compliances of a slot and a crack, 63
  condition numbers of compliance matrix, 78
  FEM and BFM, 30
  increasing number of elements, 56
  layer removal and overlapping piecewise approximation, 98
  measurement methods, 6
  plate and plate with T-joint, 60
  slitting and hole-drilling, 27
complete circumferential crack, 33, 45
complete Legendre series, 114
compliance function, 17, 39, 53, 73, 90
  for a cylinder with a radial crack, 49
compliance functions
  for 3-D bodies, 64
  initial strain functions, 150
compliance matrix, 74
  condition number, 75
  determinants, 75
  ill-conditioned, 75
  matrix norms, 75
  numerical stability, 78
compliance matrix, strip load, 83
compliance method, 17
component integrity, 3
compressive residual stress, 3
conceptually separated, 45
conductive materials, 18
consistent-splitting method, 8
continuity of rotation, 45
contour method, 8
convergency study for FEM, 58
crack compliance, 27, 33
crack compliance function, 39, 51
crack compliance method, 160
  initial strain, 138
crack propagation, 18
cut in an oblique angle, 61
cut of finite width, 16
cut with semi-circular bottom, 62

deep crack, 56, 58
deformation due to initial strain, 143
detecting surface flaw, 155
diametral cut, 132
difference
  bodies with and without the cut, 139
  circular bottom and flat bottom, 30
  crack and cut of finite width, 27
  FEM and LEFM, 57
  hole-drilling and slitting methods, 29
discontinuity across interface, 151
discretization, 25
disk, 51
displacement
  at crack mouth, 156
  on lower edge, 36
  on upper edge, 34
  produced by shear stress, 41
distributed error with alternating sign, 86
domain from 0 to 1, 73
dominant variation, 109
dye penetrant, 3, 153

edge-cracked beam, 33
edge-cracked circular body, 42
edge-cracked plate, 54
edge-creacked disk, 33
EDM
  conventional, 18
  electrode, 18
  thin wire, 101
  wire, 18
effect of residual stress, 158

eigenstrain method, 136
elastic limit
  exceed, 9
elastic modulus, 24
element mesh around the bottom of cut, 150
element mesh for semi-circular bottom, 63
elements along the circular bottom, 63
energy release rate, Irwin's classic paper, 164
equilibrium equations, 14
error
  unbalanced term, 78
error analysis, 70
error bound
  peak variation, 111
error propagation, a unit perturbance, 85
experimental validation, two-axial-cuts method and single-slice method, 133
expression
  K_I for an edge-cracked beam, 165
  K_{II} for an edge-cracked beam, 166
  for axial stress, 127
  for the axial stress in terms of hoop stress, 120
  measurement of K_I of an edge-cracked disk, 161
expressions
  in-plane stress, 14
  normal stress, 12
  shear stress, 13

face closure, 19
FE, finite element, 53
FEM, *see* finite element method
FEM, finite element method, 53
fillet weld, 59
final estimated residual stress, 108
finite element, 53
  evenly spaced, 55
  number of elements, 55
  reduction ratio, 55
finite element method, 53
  model geometry of a slot with a semicircular bottom, 147
forward substitution, 84
four-point bending, 103

Gaussian-Laguerre quadrature, 38, 191
glass
  low tensile strength, 153
graphite substrate, 151
Griffith's work, 153

high compressive stress in plastic zone in glass, 154
hole-drilling, 87
hole-drilling method, 5, 29
Hook's law, 24
hoop strain, 47
hoop strain due to a radial crack, 49
hoop stress in plane stress and plane strain, 127
horizontal displacement
  on upper edge, 34

incompatible thermal expansion coefficients, 147
inherent flaws concept, 154
inherent-strain method, 135
initial strain
  analytical solutions, 151
  axisymmetric problems, 141
  original stress computed, 146
  solution for stress in beam, 139
  two independent parts, 147
initial strain approach, 7, 17
initial strain in a beam, 139
interpolation procedure, 68, 105

Jacobi polynomials, 13, 174

laser clad and a plate, 65
laser cladding of stellite on steel, 98
layer-removal method, 5
least squares fit, 72, 74, 125
  initial strain approach, 140
least squares fit, with constraint, 131
LEFM solution, 78
LEFM, linear elastic fracture mechanics, 58
Legendre polynomial, 39, 44, 56, 58, 76, 172
Legendre polynomials, 12
Legendre-Gaussian quadrature, 192
linear elastic fracture mechanics, 33

linear superposition, 9
location
  ideal for measurement, 39
location directly opposite the cut, 41
locations inside a valve body, 101
longitudinal strip, 46

main convergence test, 105
mean between E and $E/(1-\nu^2)$, 105
measurement
  axial stress, 132
  on plane near the toe of a weld, 99
  stress intensity factor, 153
measurement error, 72
measurement of hoop stress, 98
median crack, 154
Mesnager-Sachs procedure, 117
milling, 17
minimum accuracy achievable, 110
Mode I stress intensity factor, 205
  edge-cracked disk, 177
Mode II stress intensity factor, 41
multi-pass weld, 98
multiply-connected 2-D body, 13

nonuniform width, 102
numerical integration, 189

order of approximation, 108
orthogonality, 12
over-determined linear system equation, 74
overall convergence, 107
overlapping-piecewise function, 88, 98

partial-through-thickness, 78
parts of large diameter, 129
plane strain, 24, 104
  one diameter from the end, 129
plane stress, 24
plastic zone, 154
point force solution, 51
point load solution, 19
Poisson's ratio, 24, 185
power series, 25
prescribed displacement, 9
propagation of error, 85
pyrolytic carbon coating, 151
pyrolytic carbon-coated graphite part, 146

radial deflection, 47
radial stress obtained from hoop stress, 119
random error, 94
recurrence relation, 12, 169
reduction of interval size, 88
region
  high compressive stress, 18
  high tensile stress, 18
regular element, 54
releasing residual stress, 17
residual hoop stress in the original cylinder, 128
residual stress
  compressive, 1, 3, 153
  due to shot-peening, 99
  influence on glass strength, 154
  nonuniform along the length of cut, 31
  normal stress, 11
  shear stress, 11
  tensile, 2
residual stress measurements
  several adjacent planes, 9
rigid body movement, 36, 41
ring
  hoop stress, 51
rounding-off error, 82

Saint-Venant's principle, 11, 41, 53
sawing, 17
scratching or scribing, 154
sectioning method, 5
semi-infinite plane, 20
semicircular bottom, 29
separate conceptually, 49
shape error, 112
shear stress, 31, 40
shot-peening, 3, 100, 155
SIF, *see* stress intensity factor
simply-connected 2-D body, 11
single-pass weld, 98
single-slice method, 124
  experimental validation, 131
  initial strain approach, 140
  length of specimen, 134
  residual stress in the original part after fracture, 133

slicing technique, 123
slitting method, 6, 19
  improved estimation, 29
soda-lime glass, fracture toughness, 154
solution for average strain, 162
solution for thin-walled cylinder, 48
sources of error, 70
state of deformation, plane stress or plane strain, 70
static shift, 85
strain
  due to shear stress, 61
  produced by shear stress, 41
strain at lower edge, 38
strain energy
  change due to normal stress, 34
  change due to shear stress, 40
strain gage, 17
  gage length, 17, 39
strain response to releasing residual stress, 69
stress components, on faces of cut, 16
stress intensity factor
  edge-cracked disk, 42
  Mode I for edge-cracked beam, 34
  Mode II for edge-cracked beam, 41
Stresses Due to Point Forces, beam, 167
Stresses Due to Point Forces, disk, 183
strip loading, 82
sub-surface crack, 154

T-joint weld, 59
tapered beam, 66
thermal expansion coefficient, 17
thick-walled cylinder, 50
thin specimen, 61
thin-walled non-circular part, 51
through-thickness residual stress, 103
toe of a fillet weld, 98
trepanning method, 5
truncated Legendre polynomial, 78
truncated Legendre polynomial series, 44
truncated Legendre series, 79
truncational error, 75

uncertainties, 70
unconstrained nodes, 54

varying strain gradient, 185
varying width, a part of, 64
vertical displacement
  on upper edge, 34
virtual forces, 34, 38

water-quenched bar, 131
weighted least squares fit, 81
weighted LSF, 82, 108, 114
wire EDM, 99

zero shift error, 125
zero-shift, 94

Printed in the United States